Available online at www.sciencedirect.com
SCIENCE DIRECT
Computers and Structures 84 (2006) 305–317
Computers & Structures
www.elsevier.com/locate/compstruc

Cracking behavior of RC panels subject to biaxial tensile stresses

Hyo-Gyoung Kwak *, Do-Yeon Kim

Department of Civil and Environmental Engineering, KAIST, 373-1 Guseong-dong, Yuseong-gu, Daejeon 305-701, South Korea

Received 18 November 2004; accepted 29 September 2005
Available online 6 December 2005

Abstract

An analytical model which can simulate the post-cracking nonlinear behavior of reinforced concrete (RC) members such as bars and panels subject to uniaxial and biaxial tensile stresses is presented. The proposed model includes the description of biaxial failure criteria of concrete in the tension–tension region and the average stress–strain relation of reinforcing steel. Based on strain distribution functions of steel and concrete after cracking, a criterion to consider the tension-stiffening effect is proposed using the concept of average stresses and strains. The validity of the introduced model is established by comparing the analytical predictions for reinforced concrete uniaxial tension members with results from experimental studies. In advance, correlation studies between analytical results and experimental data are also extended to RC panels subject to biaxial tensile stresses to verify the efficiency of the proposed model and to identify the significance of various effects on the response of biaxially loaded reinforced concrete panels.

Keywords: Tension-stiffening; Average stress–strain; Reinforced concrete; Biaxial tensile stresses

1. Introduction

Reinforced concrete (RC) structures are made up of two materials with different characteristics, namely, concrete and steel. Since concrete is relatively weak and brittle under tension, cracking is expected when significant tensile stress is induced in a member, and reinforcing steel is used to provide the necessary tensile strength for a structural member. In advance, because of weak tensile strength of concrete, the nonlinear response of RC structures can be roughly divided into three ranges of behavior: the uncracked elastic stage, the crack propagation of concrete and the plastic (yielding of steel or crushing of concrete) stage. The post-cracking behavior of RC structures also depends on many influencing factors (the tensile strength of concrete, anchorage length of embedded reinforcing bars, concrete cover, and steel spacing, etc.) which are deeply related to the bond characteristics between concrete and steel [13]. Accordingly, to verify the nonlinear behavior of RC structures including the bond-slip mechanism, many experimental and numerical studies have been conducted [16,32,35].

In earlier studies, characterization itself of the tension-stiffening effect due to the nonnegligible contribution of cracked concrete was the main objective. Recently, following the introduction of nonlinear fracture mechanics in RC theory [27,5], modeling of the interaction between concrete and reinforcement from the extension of fracture energy concept [22], more advanced analytical approaches have been conducted [29], Sato and Vecchio [30] and many numerical models which can implement the tension-stiffening effect into the stress–strain relation of concrete have been proposed [25,16,6]. Christiansen and Nielsen [11] presented a simple model for the prediction of plane stress behavior of reinforced concrete through determining stresses, strains and crack widths. Besides, the ACI committee 224 [1] and CEB-FIP [9] predict, in an empirical manner,

* Corresponding author. Tel.: +82 42 869 3621; fax: +82 42 869 3610.
E-mail address: khg@kaist.ac.kr (H.-G. Kwak).

0045-7949/$ - see front matter © 2005 Elsevier Ltd. All rights reserved.
doi:10.1016/j.compstruc.2005.09.020

the average stress–strain curves of a RC element subject to biaxial loadings.

Two basically different approaches have been used in considering the tension-stiffening effect by defining the strain softening part in the tension region [4,7,13]: (1) a modified stiffness approach based on a repeated modification of stiffness according to the strain history; and (2) a bond-slip based model constructed from the force equilibrium and strain compatibility condition at the cracked concrete matrix with the assumed bond stress distribution. Even though the second approach is broadly adopted in finite element formulation, there are still some limitations in application because this approach requires the assumption of bond stress distribution function along the reinforcement axis, and it follows a series of complex integration and derivation procedures to calculate the elongation and strain increment of steel and accompanying relative slip.

To address this limitation in adopting the bond-slip based tension-stiffening model, an analytical approach to predict the post-cracking behavior of RC structures subject to uniaxial or biaxial tensile stresses is introduced in this paper. Unlike previous approaches based on the assumed bond stress distribution function, the strain distribution of concrete, which is abruptly changed after cracking occurs, is defined with a polynomial function satisfying the boundary conditions at the crack face and at the inner end of the transfer length. Then, the polynomial order is determined from the energy balance condition before and after cracking. The validity of the introduced approach is established by comparing the analytical predictions for RC tension members with results from experimental and previous analytical studies. Moreover, numerical analyses for idealized RC panels subject to biaxial tensile stresses are conducted to verify the applicability of the constructed tension-stiffening model to RC containments subject to internal pressure.

2. Cracking behavior of tension member

When a symmetrical uncracked RC member is loaded in tension, the tensile force is distributed between the reinforcing steel and concrete in proportion to their respective stiffness, and cracking in concrete occurs when the stress reaches to a value corresponding to the tensile strength of concrete. In a cracked cross-section, all tensile forces are balanced by the steel encased in concrete matrix only. However, between adjacent cracks, tensile forces are transmitted from the steel to the surrounding concrete by bond forces. This effect is called the tension-stiffening effect. As shown in Fig. 1, tension-stiffening effect can be illustrated by the relation between the average stress and the average strain of an axial member through the entire range from the uncracked state to the yielding state.

During the formation of primary cracks, the average strains increase with a decrease of the stress in the concrete until a stabilized cracking state is reached (point A in Fig. 1). A continuous increase of loading results a gradual increase of the stiffness because of the bond resistance between concrete and steel, and the crack width is gradually enlarged without an additional change in the number of cracks up to reach to the yielding of reinforcing steel at the crack (point B in Fig. 1). Moreover, when the average strain along the entire length of a member reaches to the yielding strain, the stiffening effect of concrete ends at point C in Fig. 1. Fig. 1, which illustrates a typical experimental response of a RC tension member, also shows that the average stress–strain curve of reinforcing bars embedded in concrete is very different from that of the bare steel bars. First, the average yield stress of embedded steel bars f_n is significantly less than the yield stress of bare steel bars f_y and, second, the post-yield range of the average stress–strain curve of RC composite represents a more sloped line, rather than an almost horizontal plateau in bare steel bars.

From these results mentioned above, the following can be inferred: (1) the tension-stiffening model proposed in the CEB-FIP [9], which assumes the same slope of the stress–strain relation with that of the bare steel bar on the basis of no bond-slip at the post-cracking stage (A–B region in Fig. 1) overestimates the stiffness of RC structure; (2) a direct use of the stress–strain relation of bare steel bar will result in an overestimation of the post-yielding behavior of RC structures in the case of considering the tension-stiffening effect into the stress–strain relation of concrete as shown in Fig. 1(b); and (3) beyond steel yielding and up to the end of the yield plateau, the concrete matrix can contribute to the strength of a tension member through the remaining bond resistance (B–C region in Fig. 1).

If RC member is subject to tension, the reinforcing steel starts yielding close to cracks, but other volumes of steel remains elastic because of bond interaction. At this moment, the averaged yield stress must be less than the yield stress of bare bar [33,24]. Determination of the element stiffness on the basis of the yielding of steel at a cracked section at which a local stress concentration appears in the steel may cause an overestimation of the structural response at the post-yielding range. Since this phenomenon is accelerated with an increase of the deformation, the analysis of RC elements accompanying relatively large deformations requires the use of average stress–strain relations [6,29]. Accordingly, to trace the cracking behavior of RC structures up to the ultimate limit state by using the smeared crack model in which the local displacement discontinuities at cracks are distributed over some tributary area within the finite element and the behavior of cracked concrete is represented by average stress–strain relations [21], the average stress–strain relation of steel needs to be defined. Considering these characteristics related to the cracking behavior, the following average yield stress, which was introduced by Salem and Maekawa [29] from the analytical results through correlation studies with experimental data, is used in this paper to revise the monotonic envelope curve of bare steel

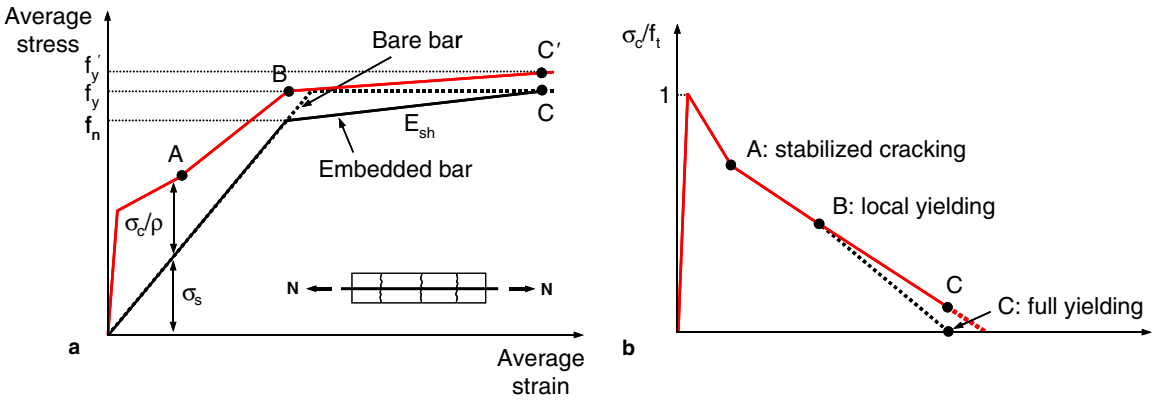

Fig. 1. Post-cracking behavior of a RC tension member: (a) average stress–strain relation of a RC tension member and (b) average stress–strain relation of concrete.

$$f_n = f_y - \delta\frac{f_t}{\rho} \tag{1}$$

where f_n is the average yield stress, f_y is the yield stress of bare bar, δ is a coefficient, f_t is the tensile strength of concrete, and ρ is the reinforcement ratio selected to be greater than the critical reinforcement ratio, $\rho_{cr} = f_t/f_y$. More details for the average stress–strain relation of steel including the hardening parameters and the average ultimate strength can be found elsewhere [29].

According to Salem's suggestion, the use of a fixed value of $\delta = 0.5$ gives reasonable estimation of the yield stress in the case of specimens with relatively small reinforcement ratio, but gives underestimation of the yield stress for the specimens with large steel ratio (see Fig. 2). Therefore, correction of the coefficient δ in Eq. (1) is accomplished in this paper by introducing the following relation, which was designed through a regression of experimental data [6,31].

$$\delta = \frac{1}{\sqrt{1 + 1.5\rho f_y}} \tag{2}$$

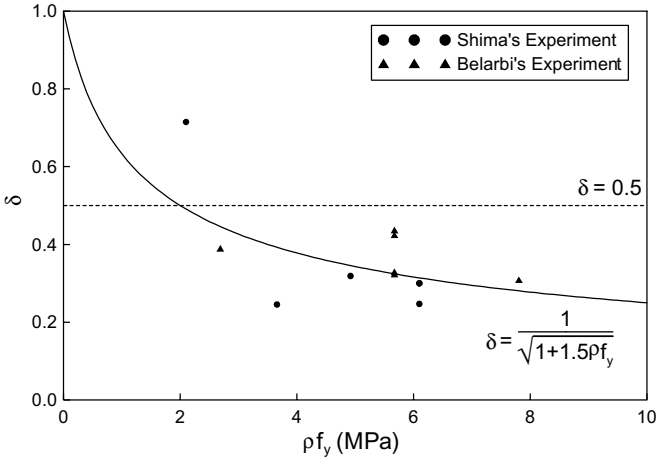

Fig. 2. Correction of coefficient δ.

3. Tension-stiffening model of uniaxial tension member

3.1. Bond-slip behavior of tension member

A part of an RC member subject to uniaxial tension is shown in Fig. 3. When the axial load N is applied, from the basic assumptions adopted, the far ends represent the fully cracked state with a steel strain of ε_{s2}. The tensile force N is transferred from the steel bar to the concrete by bond stress, and the value of the bond stress is zero at the inner end of the transfer length l_t. This means that there is no bond-slip within the central region bounded by the transfer length. Moreover, it can be assumed that the strains in steel and concrete are equal to each other at $x = l_t$, and the strain value corresponds to ε_{s1}.

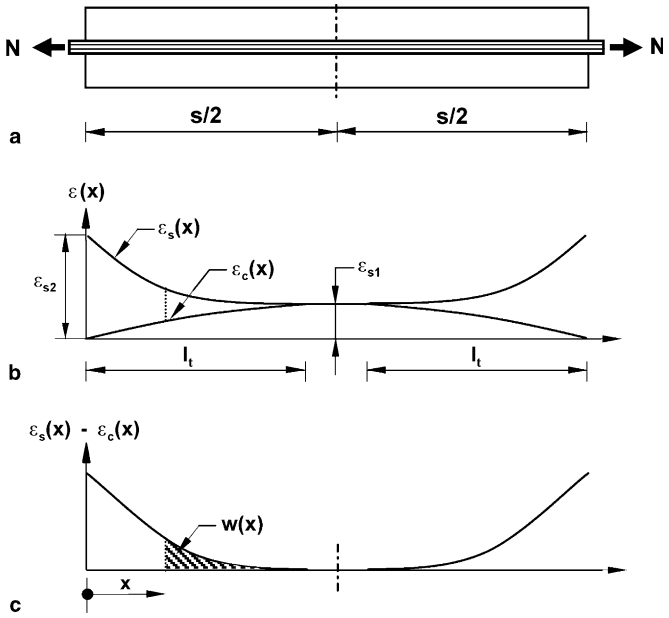

Fig. 3. Strain distribution in a part of an RC tension member: (a) tension member, (b) strain distribution and (c) strain difference.

From the strain distribution, the local slip $w(x)$ can be defined as the total difference in elongations between the reinforcement and the concrete matrix measured over the length between a distance x from a crack face and the center of the segment ($x = s/2$). That is

$$w(x) = \int_x^{s/2} (\varepsilon_s(x) - \varepsilon_c(x))\,dx \tag{3}$$

where x is the length between two adjacent cracks, which is equivalent to the crack spacing, and $\varepsilon_s(x)$ and $\varepsilon_c(x)$ are the strain distributions of steel and concrete, respectively.

On the basis of the force equilibrium and the relation of Eq. (3), the very well-known following governing differential equation for the bond-slip can be obtained [16,13]:

$$\frac{d^2 w(x)}{dx^2} - \frac{(1+n\rho)\Sigma_0}{E_s A_s} f_b(x) = 0 \tag{4}$$

where $n = E_s/E_c$, the steel ratio $\rho = A_s/A_c$, Σ_0 is the perimeter of the steel bar, f_b is the bond stress at the steel interface, and E_s and A_s are Young's modulus and sectional area of steel, respectively.

As mentioned above, the general solution of Eq. (4) is obtained in previous studies by applying the boundary conditions at the crack face and at the center of the cracked region based on an assumed bond stress distribution [32,35]. After obtaining the general solution for the bond-slip, the strain distributions of steel and concrete and corresponding bond stress along the steel axis are successively calculated using the force equilibrium and the compatibility condition at an arbitrary location [16]. However, this approach has some limitations in simulating the cracking behavior of RC axial members because it requires a series of complex integration and derivation procedures and the calculated location representing the maximum bond stress value is not coincident with that obtained from experimental study. To solve these limitations, an analytical approach on the basis of the assumed strain distribution function of concrete is introduced in this paper.

3.2. Determination of strain distributions

When the applied axial load N_1 is relatively small, the strains in steel and concrete maintain a uniform distribution with $\varepsilon_{s1} = N_1/(A_s E_s + A_c E_c)$ along the length. As the axial load (N_2) gradually increases, the strains in steel and concrete represent different distributions in the region from the crack face to the inner end of the transfer length (see Fig. 4). Moreover, the steel strain ε_{s2} at the crack face and ε_{s1} at the center of the segment become $\varepsilon_{s2} = N_2/(A_s E_s)$ and $\varepsilon_{s1} = N_2/(A_s E_s + A_c E_c)$, respectively.

From Fig. 4, the concrete strain distribution $\varepsilon_c(x)$ is assumed with a nth order polynomial function, and the steel strain distribution $\varepsilon_s(x)$ can also be expressed in terms of the concrete strain distribution function from the force equilibrium of $N_2 = \varepsilon_{s2} \cdot A_s E_s = \varepsilon_{s1} \cdot (A_s E_s + A_c E_c)$ and the relation of $\varepsilon_{s1} = \varepsilon_{c1}$. The strain distributions lead to

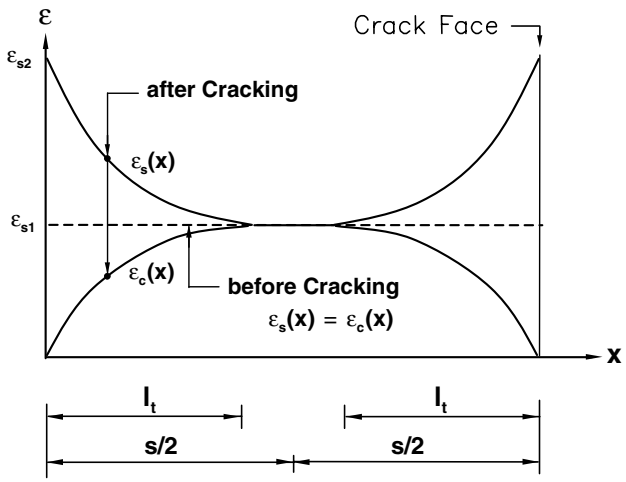

Fig. 4. Strain distribution after cracking.

$$\varepsilon_s(x) = \varepsilon_{s2} - \tfrac{1}{n\rho}\varepsilon_c(x)$$
$$\varepsilon_c(x) = \varepsilon_{s1}\left\{1 - \left(1 - \tfrac{x}{l_t}\right)^{n_c}\right\} \quad : x \leqslant l_t \tag{5a}$$
$$\varepsilon_s(x) = \varepsilon_c(x) = \varepsilon_{s1} \quad : l_t \leqslant x \leqslant s/2 \tag{5b}$$

where the area parameter $n\rho$ is in the range of 0.02–0.5 [15]. Moreover, the transfer length l_t can be determined by the following linear relationship proposed by Somayaji and Shah [32] on the basis of many experimental data for the pull-out tests:

$$l_t = K_p \frac{N_c}{\Sigma_0} \tag{6}$$

where N_c is the transfer load equal to $N_c = A_c E_c \varepsilon_{s1} = N/(1+n\rho)$, and K_p is a constant determined from the pull-out test. The experimental study by Houde and Mirza [17] indicates that the value of K_p is in the range of 1/266–1/714 in^2/lb, and the average value of 1/385 in^2/lb is used in this paper.

The strain distribution of reinforcing bar changes from the uniform distribution ε_{s1} along the segment before cracking to the assumed polynomial distribution with the strain ε_{s2} at the crack face and ε_{s1} at the inner end of the transfer length after cracking (see Fig. 4). From the energy conservation just before and after cracking at the same axial load N, the assumed polynomial order n_c can be determined because all the internal strain energy components can be represented in terms of the concrete strain with the assumed polynomial order n_c, while there is no additional external work by the axial load N just at cracking. The strain difference of steel $\varepsilon_{s2} - \varepsilon_{s1}$ means an increase of the strain energy at the reinforcing steel, ΔU_s, and that of concrete $\varepsilon_{s1} - \varepsilon_c(x)$ corresponds to a decrease of the strain energy at the concrete, ΔU_c. Moreover, the difference between ΔU_s and ΔU_c means the energy loss caused by the bond-slip, U_b. Therefore, the energy conservation can be written as

$$\Delta U_s - \Delta U_c = U_b \tag{7}$$

where

$$\Delta U_s = \int_V \Delta u_s \, dV = \int_V \int_{\varepsilon_{s1}}^{\varepsilon_s(x)} \sigma_s \cdot d\varepsilon \, dV = \frac{A_s E_s}{2} \int_0^{l_t} (\varepsilon_s(x)^2 - \varepsilon_{s1}^2) \, dx \tag{8a}$$

$$\Delta U_c = \int_V \Delta u_c \, dV = \frac{A_c E_c}{2} \int_0^{l_t} (\varepsilon_{s1}^2 - \varepsilon_c(x)^2) \, dx \tag{8b}$$

$$U_b = \Sigma_0 \int_0^{l_t} \int_0^{w(x)} \tau_b(w(x)) \, dw \, dx \tag{8c}$$

and hence

$$\frac{A_c E_c}{2} \cdot \frac{\varepsilon_{s1}\varepsilon_{s2} l_t}{2n_c + 1} = \frac{A_s E_s}{2} \cdot \frac{\varepsilon_{s1}\varepsilon_{s2} l_t}{n\rho(2n_c + 1)} = \frac{\Sigma_0 \tau_{max}}{w_1^{\alpha} \cdot (1+\alpha)} \times \frac{\varepsilon_{s2}^{1+\alpha} \cdot l_t^{1+\alpha} \cdot l_t}{(n_c+1)^{1+\alpha} \cdot ((n_c+1)(1+a)+1)} \tag{9}$$

While calculating the bond energy variation U_b, the relation of Eq. (3) and the following nonlinear bond stress-slip relation [9] are used.

$$\tau_b = \tau_{max} \cdot (w(x)/w_1)^{\alpha} \tag{10}$$

where τ_{max} is the maximum bond stress of concrete, and w_1 and α have the values of 1.0 mm and 0.4, respectively, when a very good bonding condition is maintained in a confined concrete [9].

As shown in Eqs. (8a)–(8c), all the strain energy variations are expressed with the assumed polynomial order n_c. Consequently, the order n_c can be determined through the successive iteration using the bisection method until Eq. (9) is satisfied. From the CEB-FIP [9], the coefficient α in Eq. (10) has a value between 0 and 1, and the value of n_c increases in proportional to an increase of α. Therefore, n_c must be larger than 1.0 obtained when $\alpha = 0$.

3.3. Average stress–strain relation of concrete

If the applied axial load N in a tension member reaches to 1.3 times of N_{cr} at the first crack, the specimen shows the stabilized crack pattern without additional occurrence of cracking [9,14], and the strain distribution along the member length can be represented by Fig. 5 [9]. After the crack formation has finished (point A in Fig. 1), the maximum crack spacing between adjacent cracks can be assumed to be 2.0 times of the minimum crack spacing and is equal to the transmission length l_t (length over which slip between steel and concrete occurs) [9].

From the geometric configuration for the strain distribution in Fig. 5, constructed on the basis of the assumption that the slopes in the strain distributions corresponding to S_{max} and S_{min} are the same at point A, the average strain of reinforcing steel ε_{sm}, equivalent to the mean value of the strain distributions of steel, can be calculated as

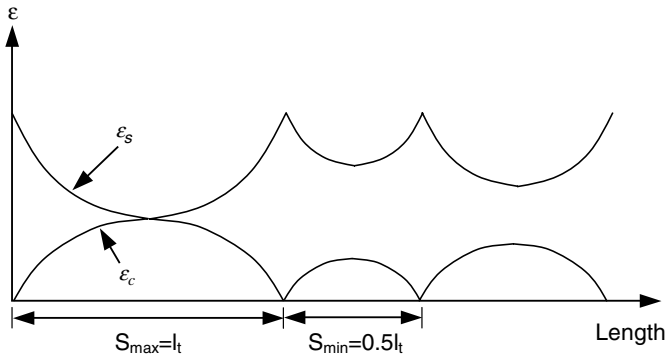

Fig. 5. Stabilized crack pattern with $S_{max} = 2S_{min}$ [9].

$$\varepsilon_{sm} = \left\{1 - \frac{3}{4} \cdot \left(\frac{n_c}{n_c+1}\right) \cdot \left(\frac{1}{1+n\rho}\right)\right\} \frac{\sigma_{s2}}{E_s} \tag{11}$$

where σ_{s2} is the steel stress at the crack face when the applied axial load has $N = 1.3N_{cr}$ and can be calculated as

$$\frac{\sigma_{s2}}{f_t} = 1.3 \cdot \left(\frac{1+n\rho}{\rho}\right) \tag{12}$$

As shown in Fig. 5, on the other hand, the strain distribution of concrete decreases with an increase of the steel strain because of the bond-slip effect but still does not consider the crack width. Accordingly, to satisfy the perfect bond assumption for the consistent displacement field between concrete and steel, the strain increment developed from the consideration of the crack width needs to be added. It might be reasonable, therefore, to assume that the average concrete strain ε_{cm} at the stabilized crack condition can be simulated by the average steel strain ε_{sm} defined in Eq. (11) [6]. With the average strain determined and the force equilibrium equation, the average stress of concrete at the stabilized crack condition can also be calculated as follows:

$$\sigma_c = \frac{\sigma_{s2}A_s - \varepsilon_{sm}E_sA_s}{A_c} \tag{13}$$

The tension-stiffening effect corresponding to an arbitrary applied axial load N_m can be defined with the strain difference between ε_{s2} and ε_{sm} ($\varepsilon_{TS} = \varepsilon_{s2} - \varepsilon_{sm}$). Moreover, the average steel strain can be represented by $\varepsilon_{sm} = \varepsilon_{s2} - 1/n\rho \cdot \varepsilon_{cm}$ from Eq. (5a), and the average concrete strain can also be expressed by $\varepsilon_{cm} = n_c/(n_c+1) \cdot \varepsilon_{s1}$ within the transfer length range when the strain distribution of $\varepsilon_{cm}(x)$ is defined with a n_cth polynomial function. Accordingly, the strain difference corresponding to the tension-stiffening effect can finally be expressed by $\varepsilon_{TS} = \varepsilon_{s2} - \varepsilon_{sm} = 1/n\rho \cdot \varepsilon_{cm}$. From this relation, the strain difference at the crack formation stage and that at the crack stabilizing stage are $\varepsilon_{TS}^{cr} = 1/n\rho \cdot n_c^{cr}/(n_c^{cr}+1) \cdot \varepsilon_{s1}$ and $\varepsilon_{TS}^{st} = 0.75/n\rho \cdot n_c^{st}/(n_c^{st}+1) \cdot \varepsilon_{s1}$, respectively. The polynomial order n_c represents different values at both stages, and the strain difference ε_{TS} must be gradually decreased as the applied axial load N increases. Namely, the strain difference at the first cracking (ε_{TS}^{cr}) must always be greater than that at the

stabilized cracking (ε_{TS}^{st}), and this condition induces the following inequality condition of:

$$0.75 \cdot \left(\frac{n_c^{st}}{n_c^{st}+1}\right) \leqslant \left(\frac{n_c^{cr}}{n_c^{cr}+1}\right) \cdot \frac{\varepsilon_{s1}^{cr}}{\varepsilon_{s1}^{st}} \tag{14}$$

Consequently, the successive iteration of Eq. (9) must be continued in the range of n_c which satisfies Eq. (14), where n_c^{cr} was already calculated from Eq. (9) and n_c^{st} is finally determined by this inequality condition. Then n_c^{st} is submitted to Eq. (11) to calculate ε_{sm} at the stabilized cracking condition.

A continuous increase of the axial load N over the stabilized cracking load leads to the yielding of reinforcing steel at the crack face while maintaining the elastic state at the other region (point B in Fig. 1). It means that the average steel stress of the embedded steel bar through the entire length will be smaller than that of the bare steel bar. A portion of the resisting capacity corresponding to the difference of yielding stress between the bare steel bar and the embedded steel bar must be carried by concrete. Therefore, the effective concrete stress σ_c and strain ε_c at point B in Fig. 1(b) can be calculated by

$$\frac{\sigma_c}{f_t} = (f_y - f_n)\frac{\rho}{f_t}, \quad \varepsilon_c = \frac{f_n}{E_s} \tag{15}$$

More increase of the axial load N finally cause the yielding of the embedded steel bar along the entire span length. To study the influence that bar yielding and large strains have on tension-stiffening, a series of RC prisms were tested by Mayer and Eligehausen [26]. As a result, the yield plateau of the bare steel bar practically disappears in the member response, since the plastic strains in the embedded steel bar are limited to the regions close to the main cracks and hardly contribute to the overall elongation. Namely, a larger axial load than that corresponding to the yielding of the bare steel bar can still be resisted in the post-yielding range of steel. On the other hand, the post-yield behavior of RC members was described as the ratio ($\varepsilon_{sn}/\varepsilon_{sr}$) between the average steel strain ε_{sn} and the steel strain ε_{sr} at the crack face with respect to ε_{sr}, as shown in Fig. 6.

As long as the concrete is uncracked, the ratio $\varepsilon_{sn}/\varepsilon_{sr}$ should be equal to 1. After abrupt drop of the ratio $\varepsilon_{sn}/\varepsilon_{sr}$ at the first cracking because of a local increase of steel strain at the crack face, it should increase again between first cracking and bar yielding. Beyond ε_y, and up to the end of the yield plateau, the ratio $\varepsilon_{sn}/\varepsilon_{sr}$ significantly reduces, until hardening is activated ($\varepsilon_{sr} = \varepsilon_{sh}$). The steep reduction is caused by the build-up of the plastic strain ε_{sr} close to the bending cracks, while the strains between the cracks are still elastic and exhibit high gradients. It means that the concrete still contributes to the strength of a tension member even after yielding of steel through the remaining bond resistance.

To take into account this contribution of concrete at the post-yielding stage, the slope of the average stress–strain relation is changed in this paper. As shown in Fig. 1(a), the slope of line B′C′, $\rho E_{sh} = \rho(f_y - f_n)/(\varepsilon_{sh} - \varepsilon_{sn})$, have been modified to the slope of line BC, $\rho(E_{sh} - (f'_y - f_n)/(\varepsilon_{sh} - \varepsilon_{sn}))$, where the stress differences $f_y - f_n$ and $f'_y - f_y$ can be assumed to be 0.89 and 0.18, corresponding to $\varepsilon_{sr} = \varepsilon_{sy}$ and $\varepsilon_{sr} = \varepsilon_{sh}$ in Fig. 6, respectively. The slope of line BC seems to be converged to $0.8\rho E_{sh}$ instead of $1.0\rho E_{sh}$, and the average stress–strain relation of concrete in the region BC is followed with the equilibrium equation.

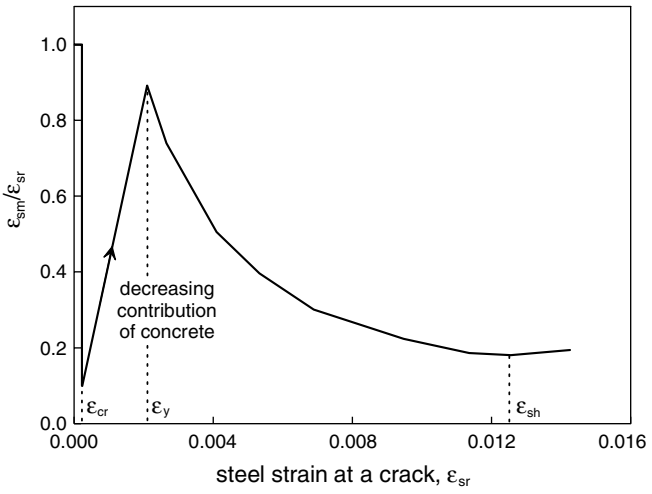

Fig. 6. Relation between ε_{sm} and ε_{sr} at post-yielding stage [26].

4. Extension of model to biaxial stresses

Unlike the reinforcing bars embedded in the concrete element, whose biaxial material properties are assumed to be simulated by the direct superposition of each element without any change in material properties, concrete under combinations of biaxial stress exhibits different strength and stress–strain behaviors from those under uniaxial loading conditions by the effects of Poisson's ratio and microcrack confinement. To simulate the change of material properties according to the biaxial tensile stress state, it is required to define the biaxial strength envelope in the tension–tension region.

Fig. 7 shows the biaxial strength envelope of concrete under biaxial tension. In contrast to a shear wall where the main part experiences a biaxial stress combination in the tension–compression region, most of wall in the containment structures subject to internal pressure experiences biaxial tensile stress combinations [20]. Accordingly, in the biaxial strength envelope in the tension–tension region is regarded to be of great importance. In this paper, the biaxial strength envelope proposed by Aoyagi and Yamada [3] is used, and the accompanying equation for the failure envelope in the tension–tension region is expressed by

$$\frac{\sigma_{1p}}{f_t} = 1 - 0.25\left(\frac{\sigma_2}{\sigma_1}\right)^2 \tag{16}$$

The tensile strength σ_{ip} in the primary direction decreases with increasing tensile stress in the other principal stress direction, and failure basically takes place by cracking in the primary direction. When the cracking occurs, however,

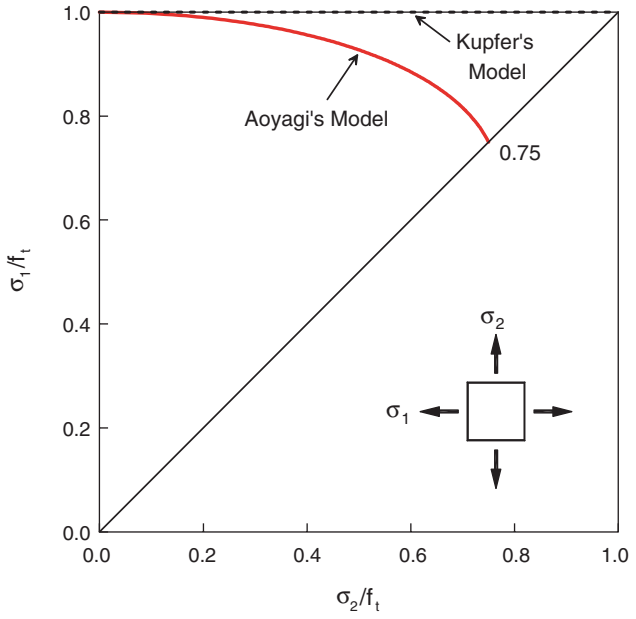

Fig. 7. Biaxial strength envelope of concrete under biaxial tension.

the principal tensile stress and strain in the other direction still remain in the ascending branch of the concrete stress–strain relation. Therefore, the proposed model introduced in this paper follows the assumption that the concrete stress–strain relation in the other direction (σ_2 direction in Fig. 7) is the same as that of uniaxial loading and does not change with the variation of tensile stress in the primary direction before concrete cracking. Using the tensile strength σ_{1p} determined from Eq. (16), the stress–strain relation of concrete in the tension part can finally defined on the basis of the uniaxial tension-stiffening model introduced in this paper (see Fig. 1).

To simulate the stress state of concrete under biaxial loading, the orthotropic model is adopted in this paper because of its simplicity and computational efficiency [12]. With reference to the principal axes of orthotropy, the incremental constitutive relation can be expressed by

$$\begin{Bmatrix} d\sigma_1 \\ d\sigma_2 \\ d\tau_{12} \end{Bmatrix} = \frac{1}{1-\nu^2} \begin{bmatrix} E_1 & \nu\sqrt{E_1E_2} & 0 \\ \nu\sqrt{E_1E_2} & E_2 & 0 \\ 0 & 0 & (1-\nu^2)\cdot G \end{bmatrix} \begin{Bmatrix} d\varepsilon_1 \\ d\varepsilon_2 \\ d\gamma_{12} \end{Bmatrix} \tag{17}$$

where E_1 and E_2 are the secant moduli of the elasticity in the direction of the axes of orthotropy, which are oriented perpendicular and parallel to the crack direction, and ν is Poisson's ratio. The most interesting feature of the material matrix of concrete in principal coordinates is the presence of the shear modulus, G, which is implying compression field theory based on the assumption that the principal concrete stress direction coincides with the principal concrete strain direction. The shear modulus can be calculated by $G = 0.5\cdot(\sigma_{c1}-\sigma_{c2})/(\varepsilon_1-\varepsilon_2)$ [10]. After cracking, if microcrack zone is fully developed, Poisson's effect disappears ($\nu = 0$).

The use of the orthotropic constitutive relation in Eq. (17) to simulate cracked concrete may not be totally realistic. In the case of a real crack, the crack surface is rough and any sliding parallel to the crack will generate some local stresses or movement normal to the crack. To properly present this type of behavior, the off-diagonal terms of the material matrix which relate shear strain with normal stress should not be zero. The relative magnitude of these off-diagonal terms decreases as the crack widens. However, this effect may not be significant in a study which focuses attention on overall structural behavior, and most researchers have neglected it [23].

The proposed concrete model accounts for progressive cracking and changes in the crack direction by assuming that the crack is always normal to the total principal strain direction (the rotating crack model). The rotating crack model which does not need shear transfer model is reasonably accurate under monotonic loading paths where principal stress does not rotate so much. More details can be found in Ref. [7]. In addition to the definition for the constitutive relations of concrete under biaxial loadings, additional modifications for the stress–strain relation of steel is also required. From the biaxial loading test for a series of orthogonally reinforced concrete panels, Pang and Hsu [28] found that there was a remarkable difference in the apparent yield stress f_n between 90° panels with the longitudinal steel oriented at 90° to the applied principal stress and 45° panels with the longitudinal steel oriented at 45°. As shown in Fig. 8, the apparent yield stresses f_n for 45° panels are lower than those for 90° panels by approximately 12%, regardless of the parameter $B = (f_t/f_y)^{1.5}/\rho$ derived by Belarbi and Hsu [6], and this reduction is attributed to the kinking of steel bars at the cracks.

When this reduction of 0.12 is applied to the equation of $f_n/f_y = 0.43 + 0.5f_y^*/f_y$, introduced by Belarbi and Hsu [6], it results the average yield strength reduction of about $0.06f_y$, f_y^* is the average apparent yield stress defined in Ref. Belarbi and Hsu [6]. In addition, Yamada's experimental results [34] also show that the maximum shear strength of RC panels occurs at 45° panels because of the

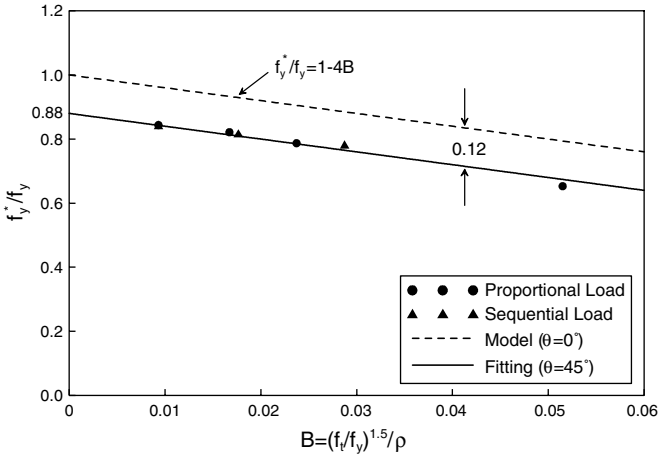

Fig. 8. Apparent yield stress of steel bars as function of parameter B [28].

Table 1
Dimensions and material properties of tension members

Specimen	Area (mm^2)	E_c (MPa)	E_s (MPa)	f_t (MPa)	f_y (MPa)	$\rho = A_s/A_c$
1	205.74×88.9	23,787	200,000	2.12	400	0.0341
2	305×178	27,794	199,955	2.62	469	0.0147
3	127×50.8	27,349	223,480	3.19	506	0.0307
4	127×50.8	27,349	191,584	3.19	508	0.0331

most dominant dowel action and its magnitude symmetrically decreases up to reach to the angle 90° between the longitudinal steel and the applied principal stress. Accordingly, to define the average stress–strain relation of steel embedded in concrete panels with an arbitrary angle θ to the applied principal stress, Eq. (1) defined for the uniaxial behavior of RC axial member has been modified as follows:

$$f_n = f_y - \delta\frac{f_t}{\rho} - 0.06 f_y\sqrt{\frac{|\theta|}{45}} \quad -45^\circ \leqslant \theta \leqslant 45^\circ \tag{18a}$$

$$f_n = f_y - \delta\frac{f_t}{\rho} - 0.06 f_y\sqrt{\frac{90-|\theta|}{45}} \quad \begin{matrix} 45^\circ < \theta \leqslant 90^\circ \\ -90^\circ \leqslant \theta < -45^\circ \end{matrix} \tag{18b}$$

On the other hand, an exact assessment of cracking in RC panels subject to general membrane stresses seems to be very difficult because of many influencing factors such as different steel ratios in both directions and changing crack angle according to the stress ratio. Most constitutive models to trace the cracking behavior of concrete, therefore, are based on the material matrix in the principal axes, using the equivalent steel ratio of $\rho_{eq}f_y = \rho_x f_y \cdot \cos^2\theta + \rho_y f_y \cdot \sin^2\theta$ [25] derived from the force equilibrium equation at the fully cracked ultimate state of a RC panel. This approach can be effectively used in concrete panels orthogonally reinforced with similar steel ratios at both directions but also has some limitations in application to other RC panels.

When the steel ratios at both directions represent a remarkable difference, the reinforcement with a smaller steel ratio will govern the tension-stiffening effect, and in advance, the post-cracking behavior of RC panels. Accordingly, for an exact simulation of the cracking behavior, it

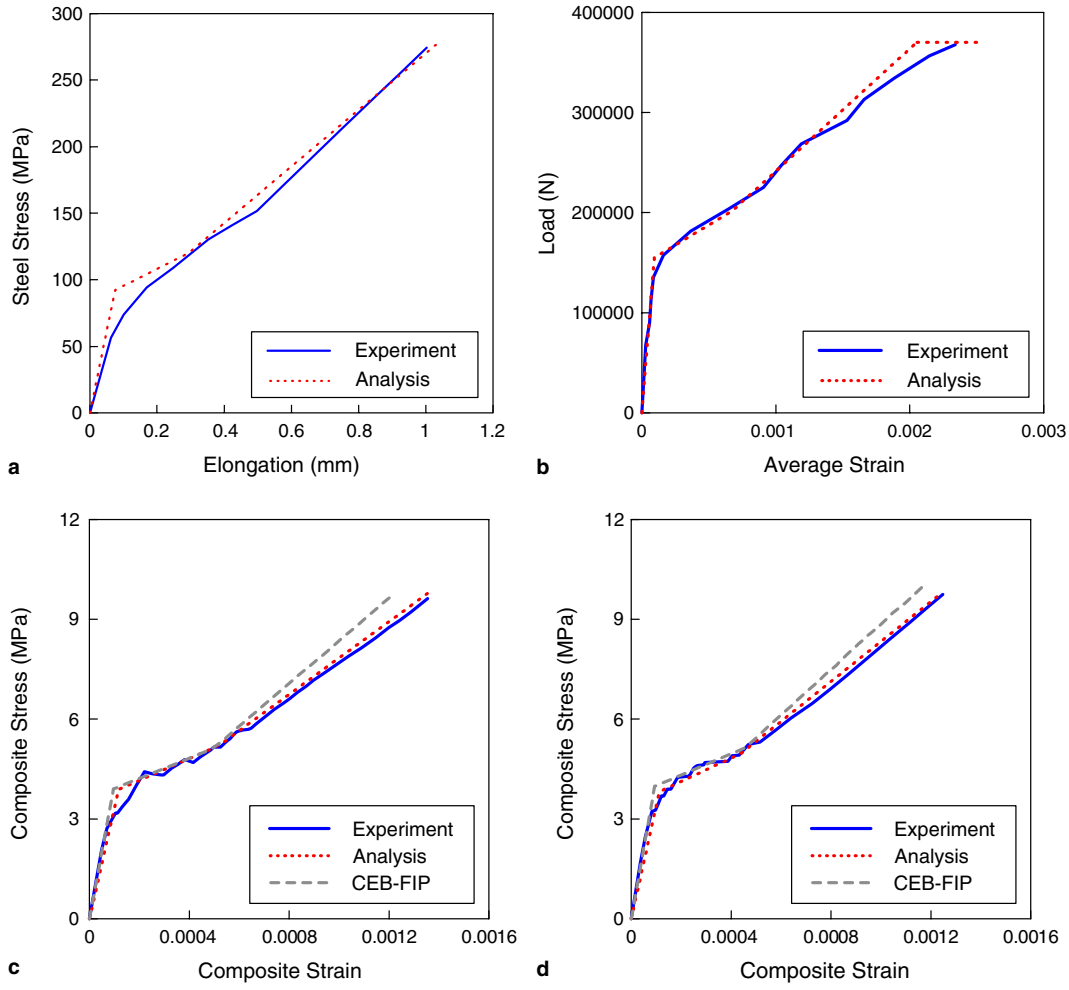

Fig. 9. Load (or stress)–elongation (or strain) relations of uniaxial members: (a) specimen 1, (b) specimen 2, (c) specimen 3 and (d) specimen 4.

might be proper to calculate the tensile stress and strain of concrete along the steel direction first, instead of the principal directions of concrete. Then, these stress and strain are transformed to the principal directions of concrete by

$$\varepsilon_{c1} = \varepsilon_x \cos^2\theta + \varepsilon_y \sin^2\theta + \gamma_{xy} \cos\theta \sin\theta \tag{19a}$$

$$\sigma_{c1} = \sum_{i}^{n} \sigma_{ci} \cos^2(\theta - \alpha_i) \tag{19b}$$

where θ is the angle between the direction normal to the crack and the global x-axis, and α_i is the orientation of reinforcement relative to the global x-axis.

5. Numerical applications

Every nonlinear analysis algorithm consists of four basic steps: formation of a current stiffness matrix, solution of equilibrium equations for the displacement increments, state determination of all elements in the model, and a convergence check. All these steps are the same with those used in the classical nonlinear analysis of RC structures. More details related to all the formulations from definition of material properties in the biaxial stress condition to the convergence check can be found in Ref. [19]. In this paper, only the efficiency of the introduced tension-stiffening model is demonstrated through correlation studies between analytical results and experimental values from idealized panel tests.

5.1. Uniaxial tension members

In order to testify the efficiency of the proposed tension-stiffening model, the cracking responses of tension members subject to direct tension are analyzed. Four kinds of tension members whose experimental results are available in the literature [17,18,27] are selected in this paper, and

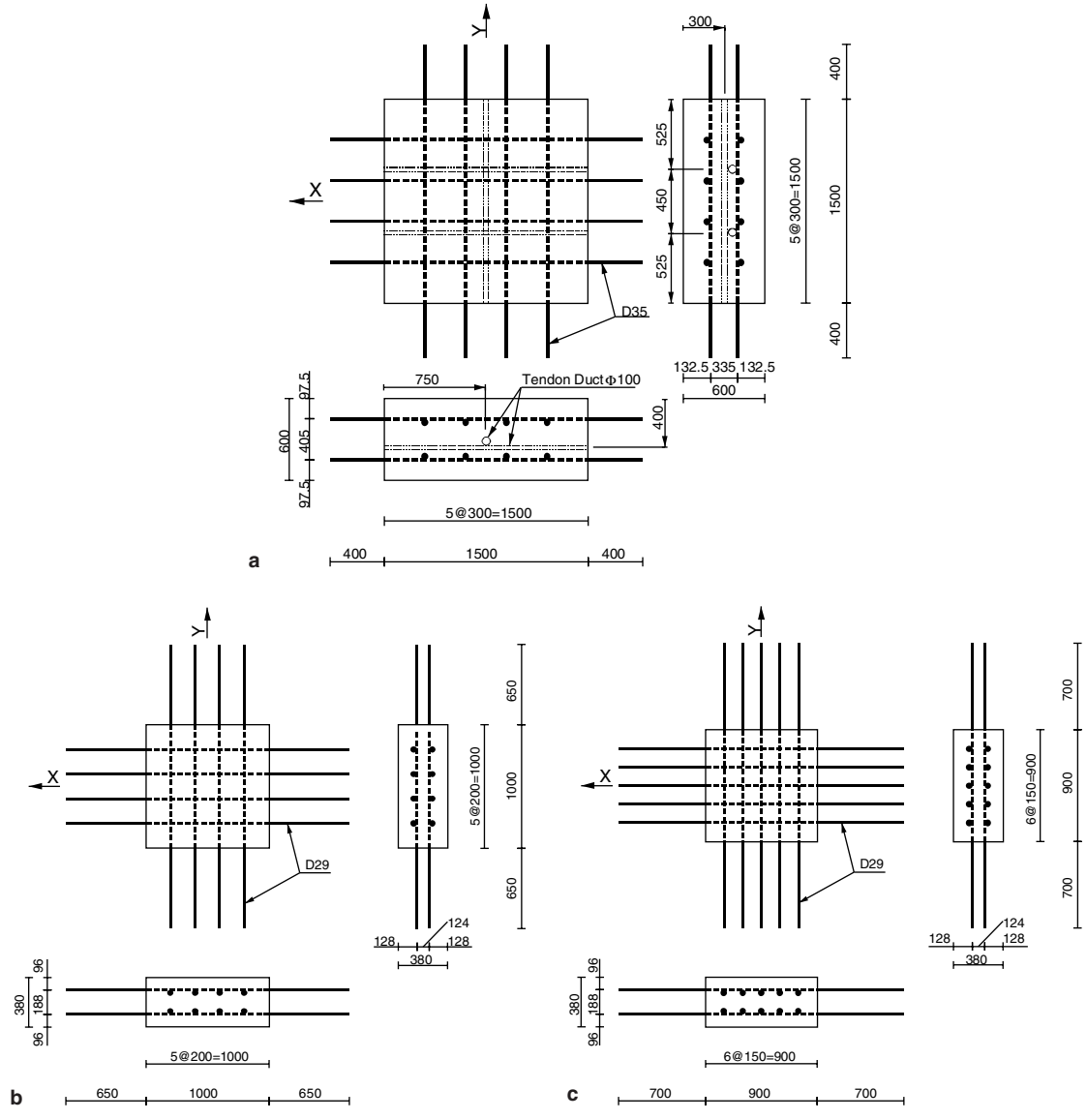

Fig. 10. Configurations and dimensions of biaxial tension specimens (dimensions in mm): (a) S40 and S60, (b) R2 and (c) R3.

the material properties of each test specimen are summarized in Table 1.

The comparison of the experimental and analytical steel stress–elongation relation of the specimen 1 (rectangular tension member) tested by Houde and Mirza [17] is shown in Fig. 9(a). In this analysis, the first crack forms at a steel stress of 94 MPa, while the stabilized cracking state appears at a steel stress of 122 MPa, which is close to the experimental results. The analytical prediction agrees well with the test results.

The prismatic member No. 7 (specimen 2) reinforced with eight bars, that was tested by Hwang and Rizkalla [18], is considered a second example. Since the reinforcement is uniformly distributed over the cross section, an almost constant stress of concrete can be expected. As shown in Fig. 9(b), the load–average strain curve is very close to the experimental results, while indicating that the introduced tension-stiffening model can predict the load–average strain behavior of a specimen through all the loading steps. As the deformation increases, the stress–elongation relation converges to that of a bare bar.

The last examples (specimens 3 and 4) are for the analyses of two reinforced concrete panels with different arrangement and size of reinforcing steel. Fig. 9(c) and Fig. 9(d) shows comparison between the experimentally measured and numerically predicted stress–strain curves with that calculated by CEB-FIP [9] model. As shown in these figures, CEB-FIP model overestimates the concrete contribution at large strain stage, while the proposed model provides good agreement with the experimentally measured curves. The four preceding examples show that analysis of a reinforced concrete member under tensile loading using the introduced approach is valid. The predictions of crack loads, stabilized crack point, and the stress–elongation relation are satisfactory when compared with test results.

5.2. RC panels subject to biaxial tension

To verify the applicability of the introduced numerical model in simulating the behavior of RC structures subject to biaxial tension, such as containment walls of nuclear power plants, correlation studies between analytical predictions and experimental results are carried out for RC panels tested in the Korea Atomic Energy Research Institute (KAERI) [8]. Among the tested panels, representative four panels of S40, S60, R2 and R3 are selected, and the specimen dimensions are 1500 mm × 1500 mm × 600 mm for S40 and S60, 1000 mm × 1000 mm × 380 mm for R2, and 900 mm × 900 mm × 380 mm for R3. As shown in Fig. 10, reinforcements are orthogonally placed, and the biaxial tension loads directly act to the reinforcement. The loading ratio and material properties of each panel are summarized in Table 2.

Panels are modeled with a single four-node element because of the uniformity of the strain and stress fields (see Fig. 11). The analytical predictions of the proposed model at four test panels are compared with the experimental average stress–strain relations obtained from LVDT measurements. As shown in Fig. 12, the cracking stresses and failure stresses from the numerical analyses agree fairly well with those of the experimental results. Because the global behavior is governed by the stress–strain relation in the hoop direction, the existence of considerable stiffness at the end of the calculation in the meridional direction can be ignored. It can thus be concluded that the structural behavior of orthogonally reinforced concrete panels subject to biaxial tension is effectively simulated by the introduced analytical model.

5.3. RC panels with inclined reinforcement and subject to uniaxial tension

To testify the applicability of the proposed model to RC panels with general reinforcement configurations,

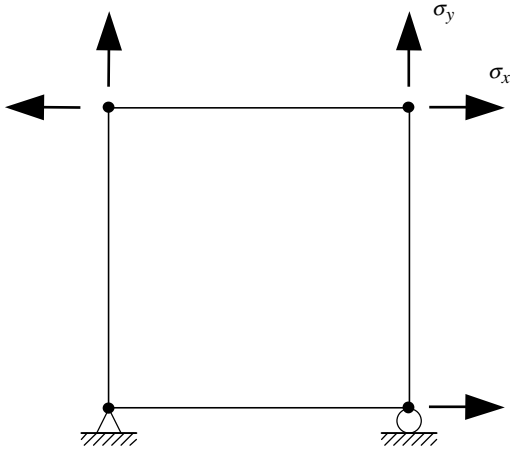

Fig. 11. Finite element idealization of RC panel.

Table 2
Loading ratios and material properties of biaxial tension panels

Panel	Loading (σ_x:σ_y)	f_t	E_c	$\rho_x = \rho_y$	f_y	E_{s1}	E_{s2}	d_b (mm)
S40	2:1	2.1	28,328	0.0085 (0.0105[a])	410	205,744	$0.02E_{s1}$	35
S60	2:1	2.4	29,435					
R2	1:1	2.1	27,477	0.0135	404	194,413	$0.02E_{s1}$	29
R3	1:1			0.0188				

Unit: MPa, $f_t = 0.33(f'_c)0.5$.
[a] Effective reinforcement ratio.

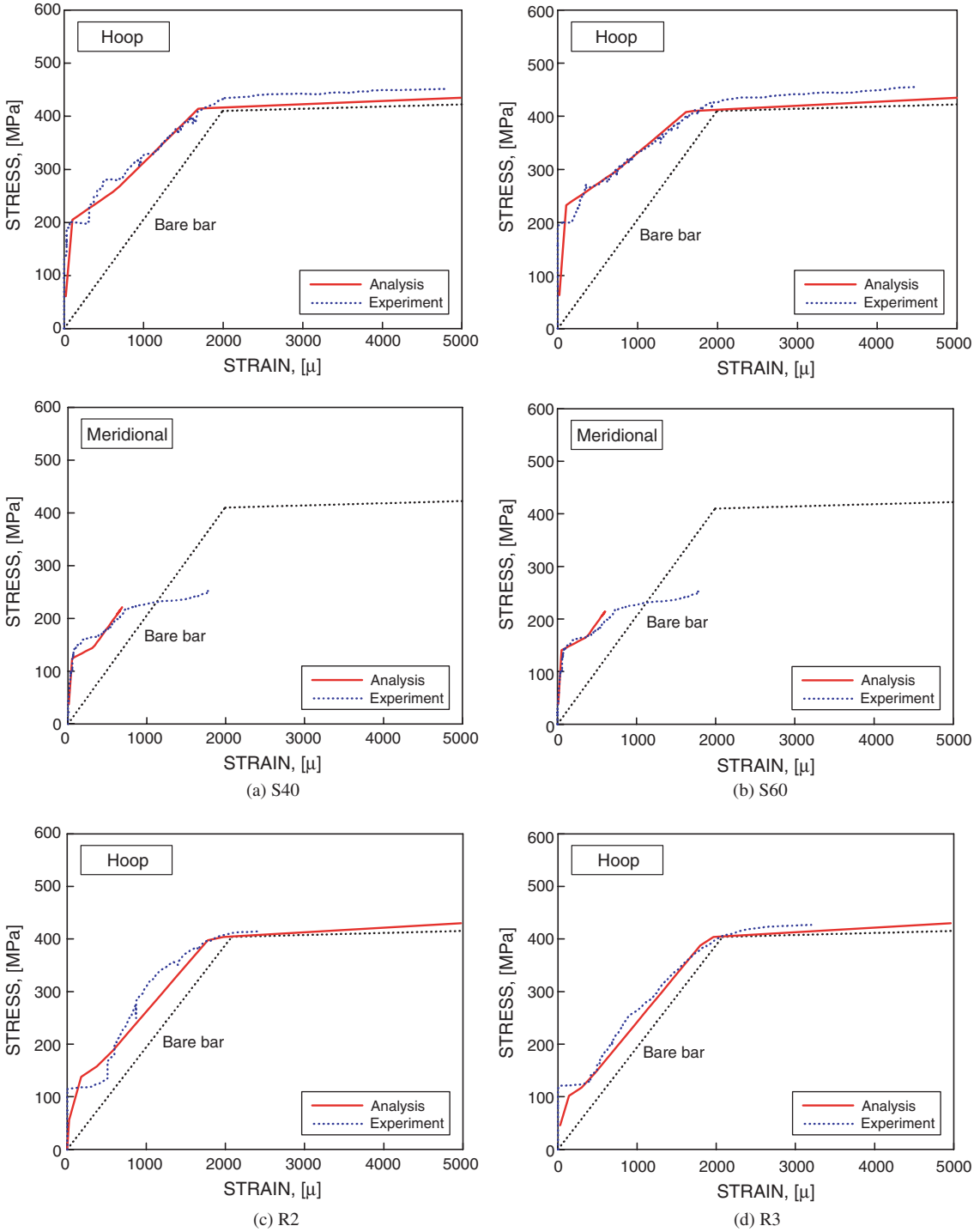

(a) S40 (b) S60

(c) R2 (d) R3

Fig. 12. Average stress–strain curves of biaxial tension specimens.

RC panels tested by Aoyagi [2], orthogonally reinforced but loaded by in-plane forces inclined to the directions of reinforcements are analyzed.

Because of a limitation in obtaining the experimental data, only Nos. 22, 23 and 26 specimens are considered in this paper. As shown in Fig. 13, the panel specimens subject to uniaxial tensile stress were 1500 mm square and 100 mm thick, and were identically reinforced in both directions. Reinforcements were arranged at $\theta = 0°$, 22.5°, and 45° with respect to the applied loading direction. The reinforcement ratios in both directions along defined on a section perpendicular to the reinforcing bar are 1.183%. The material properties of concrete and steel used in the analyses are: $f'_c = 25$ MPa, $f_t = 0.33(f'_c)^{0.5}$ MPa, $E_c = 2 \times 10^4$ MPa, $f_y = 371$ MPa, and $E_s = 2 \times 10^5$ MPa. Since the entire region represents the same stress condition, only one four-node element is used, as in the previous example.

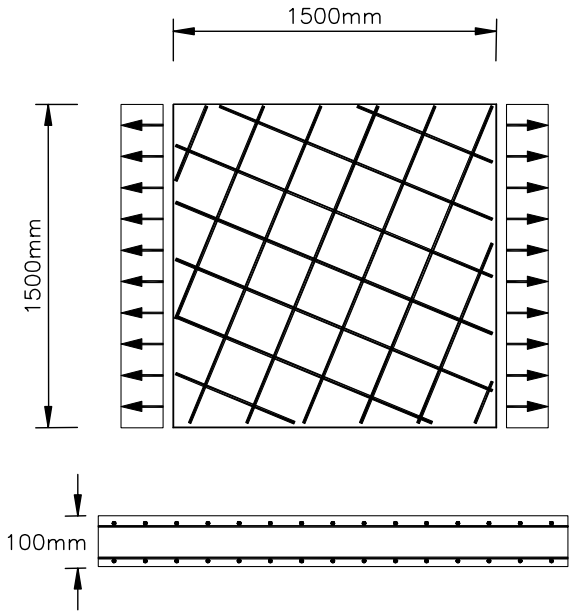

Fig. 13. RC panel specimen with inclined reinforcement.

Fig. 14 shows comparisons of measured average deformations in the direction of the principal tensile force N_1 with the results obtained by the proposed model for the cases of $\alpha = 0°$, 22.5°, and 45°. The deformations increase in proportional to the deviation angle α and can also be predicted fairly well by the analytical procedure proposed in this paper. In advance, the average steel strain to the applied load N_1, experimentally obtained at the specimen No. 23, is also compared with that calculated by the proposed analytical model in Fig. 15. Even though the model prediction in the *j*-direction relatively underestimates the steel stiffness after cracking, it does not exert a great influence upon the overall response governed by the behavior of steel in the *i*-direction.

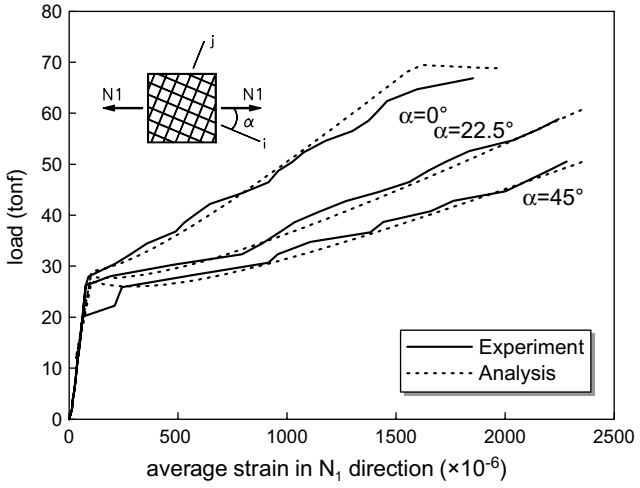

Fig. 14. Load–average strain relations in N_1 direction.

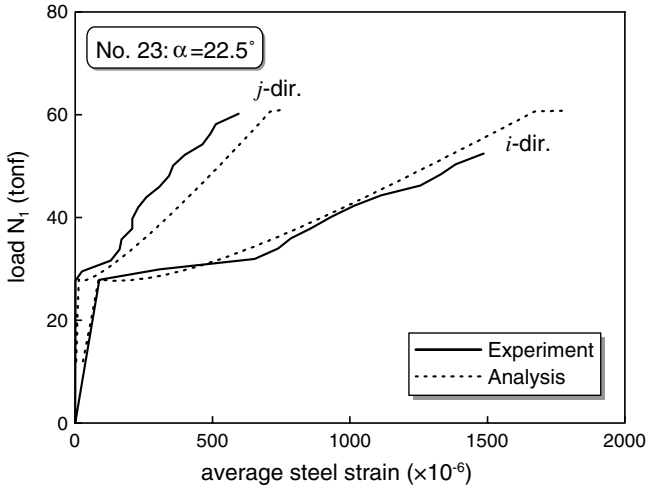

Fig. 15. Comparison of measured average strains with calculated ones in steels.

6. Conclusions

In this paper, an analytical model which can simulate the post-cracking behavior of an RC tension member subject to biaxial tension is proposed. Instead of using the assumed bond stress distribution, the concrete strain distribution with *n*th order polynomial function is assumed and the polynomial order is determined on the basis of the energy balance before and after cracking. The effective concrete stress–strain relation at a limit state is also derived from the average steel stress of the embedded steel bar. In advance, the tension-stiffening model developed in the uniaxial tension member is extended to the biaxial tension member.

By adopting the proposed model, the post-cracking behavior of RC structures subject to uniaxial or biaxial tension can be effectively analyzed without any additional complex calculation. The efficiency and reliability of the proposed model are demonstrated through application examples of biaxially loaded RC panels.

Acknowledgement

The research reported in this paper was made possible by the financial support from the Smart Infra-Structure Technology Center funded by the Korea Science and Engineering Foundation. The authors would like to express their gratitude to this organization for the financial support.

References

[1] ACI Committee 224. Cracking of concrete members in direct tension. ACI 224.2R-92, Detroit: American Concrete Institute; 1992.
[2] Aoyagi Y. Estimate of strength and deformation characteristics of reinforced concrete shell elements subjected to in-plane forces. Finite Element Anal Reinf Concr Struct, ASCE 1985:602–19.

[3] Aoyagi Y, Yamada K. Strength and deformation characteristics of reinforced concrete shell elements subjected to in-plane forces. Proc JSCE 1983(331):167–80.
[4] ASCE task committee on finite element analysis of reinforced concrete structures. State-of-the-art report on finite element analysis of reinforced concrete, New York: ASCE; 1982.
[5] Barros MHFM, Martins RAF, Ferreira CC. Tension-stiffening model with increasing damage for reinforced concrete. Eng Comput 2001;18(5–6):759–85.
[6] Belarbi A, Hsu TTC. Constitutive laws of concrete in tension and reinforcing bars stiffened by concrete. ACI Struct J 1994;91(4): 465–74.
[7] CEB. RC elements under cyclic loading: state of the art report. London: Thomas Telford Services Ltd; 1996.
[8] Chung WK. Prestressed concrete containment structural element test. Daejeon: Korea Atomic Energy Research Institute; 2000. KAERI CM-420.
[9] Comité Euro-International du Béton. CEB-FIP model code 1990. London: Thomas Telford Service Ltd; 1993.
[10] Crisfield MA, Wills J. Analysis of *R/C* panels using different concrete models. J Eng Mech ASCE 1989;115(3):578–97.
[11] Christiansen MB, Nielsen MP. Plane stress tension-stiffening effects in reinforced concrete. Mag Concr Res 2001;53(6):357–65.
[12] Darwin D, Pecknold DA. Nonlinear biaxial stress–strain law for concrete. J Eng Mech Div ASCE 1977;103(EM2):229–41.
[13] FIB. Bond of reinforcement in concrete, state-of-art report prepared by task group bond models. International federation for structural concrete (FiB), Lausanne; 2000.
[14] FIB. Structural concrete: textbook on behavior, design and performance. Bulletin No. 1, FIB, Switzerland; 1999.
[15] Gerstle W, Ingraffera AR, Gergely P. Tension-stiffening: a fracture mechanics approach, bond in concrete. London: Applied Science Publishers; 1978.
[16] Gupta AK, Maestrini SR. Tension-stiffness model for reinforced concrete bars. J Struct Eng ASCE 1990;116(3):769–90.
[17] Houde J, Mirza MS. A study of bond stress-slip relationship in reinforced concrete. Structural concrete series no. 72-8, Montreal, Quebec: McGill University; 1972.
[18] Hwang LS, Rizkalla SH. Behavior of reinforced concrete in tension at post-cracking range,'' Engineering Report, Department of Civil Engineering, Winnipeg: University of Manitoba; 1983.
[19] Kwak HG, Filippou FC. Finite element analysis of reinforced concrete structures under monotonic loads. Berkeley: University of California; 1990. UCB/SEMM-90/14.
[20] Kwak HG, Kim DY. Nonlinear analysis of RC shear walls considering tension-stiffening effect. Comput Struct 2001;75(5): 499–517.
[21] Kwak HG, Song JY. Cracking analysis of RC members using polynomial strain distribution function. Eng Struct 2002;24(4): 455–68.
[22] Lackner R, Mang HA. Scale transition in steel–concrete interaction. I: model. J Eng Mech ASCE 2003;129(4):393–402.
[23] Lin CS, Scordelis AC. Nonlinear analysis of RC shells of general form. J Struct Div ASCE 1975;101(ST3):523–38.
[24] Maekawa K, Pimanmas A, Okamura H. Nonlinear mechanics of reinforced concrete. London: Spon Press; 2003.
[25] Massicotte B, Elwi AE, MacGregor JG. Tension-stiffening model for planar reinforced concrete members. J Struct Eng ASCE 1990; 116(11):3039–58.
[26] Mayer U, Eligehausen R. Bond behavior of ribbed bars at inelastic steel strains. In: Proceedings of 2nd International Ph.D. Symposium in Civil Engineering. Hungary: Technical University of Budapest; 1998. p. 39–46.
[27] Ouyang C, Wollrab E, Kulkarni SM, Shah SP. Prediction of cracking response of reinforced concrete tensile members. J Struct Eng ASCE 1997;123(1):70–8.
[28] Pang XB, Hsu TTC. Behavior of reinforced concrete membrane elements in shear. ACI Struct J 1995;92(6):665–79.
[29] Salem H, Maekawa K. Spatially averaged tensile mechanics for cracked concrete and reinforcement in highly inelastic range. Concr Lib JSCE 1999(34):151–69.
[30] Sato Y, Vecchio F. Tension stiffening and crack formation in RC members with Fiber reinforced polymer sheets. J Struct Eng ASCE 2003;129(6):717–24.
[31] Shima H, Chou L, Okamura H. Micro and macro models for bond in RC. J Fac Eng Univ Tokyo (B) 1987;39(2):133–94.
[32] Somayaji S, Shah SP. Bond stress versus slip relationship and cracking response of tension members. ACI Struct J 1981;91(4): 465–74.
[33] Stevens NJ, Uzumeri SM, Collins MP. Reinforced concrete subjected to reversed cyclic shear-experiments and constitutive model. ACI Struct J 1991;88(2):135–46.
[34] Yamada K, Aoyagi Y. Shear transfer across cracks. In: Proceedings of JCI 2nd Colloquium on Shear Analysis of RC Structures, JCI; 1983. p. 19–28.
[35] Yang S, Chen J. Bond slip and crack width calculation of tension members. ACI Struct J 1988;85(7):414–22.